Supporting Information for: "Structural hierarchies define toughness and defect-tolerance despite simple and mechanically inferior brittle building blocks"

Dipanjan Sen[1,2] & Markus J. Buehler[1]*

[1] *Laboratory for Atomistic and Molecular Mechanics, Department of Civil and Environmental Engineering, 77 Massachusetts Ave. Room 1-235A&B, Cambridge, MA, USA*

[2] *Department of Materials Science and Engineering, Massachusetts Institute of Technology 77 Mass. Ave., Cambridge, MA 02139, USA*

** Corresponding author, e-mail: mbuehler@MIT.EDU*

1. Detailed methods

A multiscale bottom-up computational methodology is used here to study the effect of hierarchical design on material properties and the mechanics of deformation. The development and validation of the mesoscale method is covered in another work [1], but is reproduced here for continuity. At the nanoscale we use molecular dynamics simulations to study the mechanics of the nanoporous silica structures. Molecular dynamics with the first principles based reactive ReaxFF atomistic force field is a powerful tool to capture fundamental nanoscale phenomena and the mechanisms behind them. At the micron length scale, we develop a mesoscale spring-lattice network model. The model is derived from as well as validated against the atomistic results. Spring-lattice network models at the micron length scale are able to capture elasticity, plasticity and fracture phenomena at these length scales. We describe the details of the methods in the following sections.

1.1. *ReaxFF force field*

At the nanoscale we use the first-principles derived ReaxFF force field (for details see [2]) to characterize the mechanical behavior of nanoporous silica structures. The ReaxFF description is based on a bond-length bond-order description and fitted to density-functional calculations of energy landscapes of bond-distortion, breaking and forming events. A variety of Si-O clusters are used for fitting parameters, as also energetics of bulk crystalline phases of silicon and silica under tension and compression. The ReaxFF potential has been used successfully in predicting fracture phenomena in silicon and silica [3-5], and interfacial structure at silicon/silica interfaces [6, 7].

Fully-atomistic simulations have recently been carried out for the mechanics of nanoporous silica structures [8]. The studies show the effect of pore size, distribution and porosity on elastic modulus, plasticity, ductility and toughness of the structures. Figure S1(a) shows one of these characteristic nano-honeycomb silica structures. The availability of these studies allows us to extract constitutive laws of nanoporous silica behavior that can be used to build mesoscale models of silica structures with hierarchies.

1.2. *Mesoscale method development and validation*

Figure S1(b) shows the model setup consisting of a network of material particles connected in a lattice arrangement through springs. Such two-dimensional spring-lattice networks have been used previously to model deformation and fracture in brittle and quasi-brittle materials [9-12], and are particularly suitable for studying fracture phenomena in heterogeneous materials [13-15]. The two-dimensional

nature of the model resembles plane strain loading conditions. The constitutive stress-strain law under tensile load is obtained for a particular nano-honeycomb silica and bulk silica using atomistic simulations, shown in Figure S1(c). In this figure, the bulk silica structure has a pre-crack with dimensions of the pore size in the nano-honeycomb structure, to compare structures with similar defect sizes.

As seen in Figure S1(c), the bulk structure is stiff and brittle, while the nanoporous structure is soft and ductile. The force-extension law for the mesoscale inter-particle potential is hyperelastic and is fit to the constitutive law behavior of nano-silica and bulk silica under tensile load (Figure S1(d)). The hyperelastic spring potential models the atomistic results for the nano-honeycomb as elastic-perfectly plastic behavior, and the bulk silica as elastic-brittle behavior. For the nano-honeycomb, the flow stress is obtained from atomistic simulations, and is calculated as the mean stress during plastic deformation. Since the aim of this study is to obtain mechanics of different composite structures, the properties of the local springs in the lattice in a certain material model are changed according to whether they lie geometrically inside the matrix or reinforcing phase.

The brittle bulk silica phase inter-particle potential is modeled as follows:

$$F_A\left(\Delta L_A\right)=\begin{cases} k_A \Delta L_A & \text{if } \Delta L_A < \Delta L_{A,c}, \\ 0 & \text{if } \Delta L_A > \Delta L_{A,c}, \end{cases} \tag{1}$$

where F_A is the force on a spring between two material particles of the brittle phase, k_A is the force constant for the spring, ΔL_A is the extension in the spring, and $\Delta L_{A,c}$ is the critical cutoff distance for the spring. The cutoff distance $\Delta L_{A,c}$, beyond which the mesoscale spring carries zero load, is fixed based on the failure strain, and the force constant k_A is fit to the elastic modulus of the material obtained from atomistic simulations.

The ductile nano-porous phase inter-particle potential is modeled as:

$$F_B\left(\Delta L\right)=\begin{cases} k_B \Delta L_B & \text{if } \Delta L_B < \Delta L_{B,1}, \\ k_B \Delta L_{B,1} + k_C\left(\Delta L_B - \Delta L_{B,1}\right) & \text{if } \Delta L_{B,1} < \Delta L_B < \Delta L_{B,c}, \\ 0 & \text{if } \Delta L_B > \Delta L_{B,c}, \end{cases} \tag{2}$$

where F_B is the force on a spring between two material particles of the ductile phase, ΔL_B is the extension in the spring, and $\Delta L_{B,1}$ is the extension for the spring for the onset of the plastic regime, and $\Delta L_{B,c}$ is the critical cutoff extension when the spring breaks and stops carrying load, k_B is the force constant for the elastic response, and $k_C = k_B/100$ is a small force constant to model plastic deformation at constant flow stress. The parameter $\Delta L_{B,1}$ is fit to the yield strain, and $\Delta L_{B,c}$ is fit to the failure strain, and k_B is fit to the elastic modulus for the nano-honeycomb structure obtained from the atomistic simulations (Figure S1(c)).

The mesoscale model uses a triangular lattice regular mesh for the arrangement of the springs. This results in isotropic elasticity behavior which can be assumed if the underlying structure is polycrystalline with regular arrangement of grains. Anisotropic behavior could also be introduced in the mesoscale model in principle, but for the proof-of-concept study targeted in this paper (in the spirit of simple computational experiments), we assume isotropic behavior in the underlying atomistic structure. The implications of this assumption are that crystal-orientation dependent anisotropic elastic

and fracture behavior phenomena will not be captured through this model. The interfaces between the two phases in the composite, if the crystal structure is not continuous across the interface, would also possibly contribute to plasticity in the material through slip and friction, however the interfaces have been just assigned the low strength and stiffness values of the nanoporous phase in the model. This does not allow for the model to capture any toughness enhancement by interfacial plasticity mechanisms.

Bulk two-dimensional mesoscale models are constructed of bulk silica and nanoporous silica and subject to tensile testing. Comparison of the elastic moduli and fracture toughness between the atomistic simulations and mesoscale simulations are used to fix spring constants and inter-particle distance in the mesoscale model.

The elastic modulus and fracture toughness for the atomistic model are calculated for a bulk silica sample with a centre-crack. The fracture toughness using the ReaxFF force field for silica is calculated to be $0.79\ \mathrm{MPa}\sqrt{\mathrm{m}}$. This is rather close to experimental values in the literature for fused quartz, 0.6-0.75 $\mathrm{MPa}\sqrt{\mathrm{m}}$ [16, 17]. The elastic modulus for the spring-lattice model is fit to 102.3 GPa and the mode I fracture toughness to be $0.79\ \mathrm{MPa}\sqrt{\mathrm{m}}$.

To match the atomistic simulation value, an inter-particle distance of 78 nm and spring constants of 3,932 N/m and 134.4 N/m for the brittle and ductile phases, respectively, are chosen for a through thickness of 100 nm. This ensures for a separation of scales between the scales described by the atomistic model and the characteristic length-scale associated with the mesoscale model (the typical scales of the atomistic-level models is up to ten nanometers). It is noted here that the model parameters can easily be adapted to describe other nanostructures, and can even be extended to describe multiple nanostructures in the study of hierarchical systems. The specific model considered here represents one specific case study explored here.

1.3. *Fracture property characterization*

For materials that show failure by growth of a single dominant crack, we characterize them by calculating their fracture toughness. The toughness is calculated by calculating the energy release rate by invoking the J-integral [18, 19] in its domain form [20] around the crack tip, given by:

$$J = \int_{S_0} \sum_{i,j}^{2} \left[\left(W\delta_{2j} - P_{ij} \frac{\partial u_i}{\partial X_2} \right) \frac{\partial q}{\partial X_j} \right] dS, \tag{3}$$

where W is the strain energy density, P_{ij} is the first Piola-Kirchoff stress tensor, u_i represents the displacement field, X are the material coordinates, S_0 represents the undeformed area of the domain, δ is the Kronecker delta, and

$$q = \begin{cases} 0: & r = r_1, \\ 1: & r = r_2, \\ (r - r_1)/(r_2 - r_1): & r_1 < r < r_2, \end{cases} \tag{4}$$

where the parameters r_1 and r_2 are shown in Figure S2. The discrete form of this equation, for small displacements, is given by (see, e.g. [21, 22]):

$$J = \sum_{\alpha \in S_0} \sum_{i,j}^{2} \left[\left(W^{\alpha}\delta_{2j} - P_{ij}^{\alpha} \frac{\partial u_i}{\partial X_2} \right) \frac{\partial q(X_{\alpha})}{\partial X_j} \right] S_0^{\alpha}, \tag{5}$$

where S_0^α is the initial undeformed area occupied by the material particle α, X_α is the initial position of material particle α, W^α is the local strain energy density at any material particle α which is calculated as follows,

$$W^\alpha = \frac{1}{S^\alpha}\left(\phi^\alpha\left(\varepsilon_{ij}\right) - \phi^\alpha(0)\right), \tag{6}$$

where ϕ^α is the potential strain energy of the material particle α, obtained from simulation by splitting the spring potential energy between material particles sharing the spring bond, and the stress at the atom $\alpha\left(P_{ij}^\alpha\right)$ is calculated from the virial theorem [23]:

$$\mathrm{P}^\alpha = \frac{1}{2\Omega_\alpha}\sum_{\beta\neq\alpha}\mathrm{r}^{\alpha\beta}\otimes\mathrm{f}^{\alpha\beta}, \tag{7}$$

where $\mathbf{r}^{\alpha\beta}$ is a vector joining material particles α and β, $\mathbf{f}^{\alpha\beta}$ is the force applied on material particle α by material particle β, and $\Omega_\alpha = S^\alpha t$ is the volume occupied by material particle α, where S^α is the area occupied by the material particle α in the deformed configuration. This formulation of the J-integral is used to avoid involving high stress values at the crack tip region in the calculation, and the convergence of the J-integral is checked by measuring its value against different integration domain regions. The strain ε_{ij}^α, and $\partial u_i/\partial X_1$ are obtained by a local least square fit to the neighbor displacement field at each material particle location.

1.4. *R-curve calculation*

Stable crack advance for every load configuration is noted by finding the crack tip location. A particular spring bond is regarded as broken when its deformation exceeds the cutoff for the interaction. Crack surfaces are visualized by finding all spring bonds which have snapped for a given load. The J-integral is used to find the energy release rate for a given amount of stable crack advance. Plot of the J-integral from the start of crack initiation through crack propagation provides the R-curve [24] for the material, *i.e.* how its fracture toughness changes as a function of stable crack advance.

J-integral calculations for different structures are done with large initial crack sizes. In all cases the initial cracks are chosen large enough to prevent a diffuse micro-cracking response in the entire material, as this would prevent us from carrying out the calculation of the J-integral through the method demonstrated above, due to unavailability of an integration region free of cracks.

2. Supporting References

1. Sen, D. and M.J. Buehler, *Atomistically-informed mesoscale model of deformation and failure of bioinspired hierarchical silica nanocomposites.* International Journal of Applied Mechanics, 2010. **2**(4): p. 699-717.
2. Van Duin, A.C.T., A. Strachan, S. Stewman, Q. Zhang, X. Xu, and W.A. Goddard III, *ReaxFFSiO reactive force field for silicon and silicon oxide systems.* J. Phys. Chem. A, 2003. **107**(19): p. 3803-3811.
3. Buehler, M.J., A.C.T.v. Duin, and W.A. Goddard, *Multi-paradigm modeling of dynamical crack propagation in silicon using the ReaxFF reactive force field.* Phys. Rev. Lett., 2006. **96**(9): p. 095505

4. Buehler, M.J., H. Tang, A.C.T. van Duin, and W.A. Goddard III, *Threshold crack speed controls dynamical fracture of silicon single crystals.* Physical Review Letters, 2007. **99**(16): p. 165502.
5. Garcia, A.P. and M.J. Buehler, *Bioinspired nanoporous silicon provides great toughness at great deformability.* Computational Materials Science, 2010. **48**(2): p. 303-309.
6. Yilmaz, D.E., C. Bulutay, and T. Çagin, *Pathways of bond topology transitions at the interface of silicon nanocrystals and amorphous silica matrix.* Physical Review B, 2008. **77**(15): p. 155306.
7. Yilmaz, D.E., C. Bulutay, and T. Çagin, *Analysis of strain fields in silicon nanocrystals.* Applied Physics Letters, 2009. **94**: p. 191914.
8. Garcia, A.P., D. Sen, and M.J. Buehler, *Hierarchical silica nanostructures inspired by diatom algae yield superior deformability, toughness and strength.* Metallurgical and Materials Transactions A, 2011.
9. Carpinteri, A., B. Chiaia, and S. Invernizzi, *Numerical analysis of indentation fracture in quasi-brittle materials.* Engineering Fracture Mechanics, 2004. **71**(4-6): p. 567-577.
10. Ostoja-Starzewski, M., *Lattice models in micromechanics.* Applied Mechanics Reviews, 2002. **55**: p. 35-60.
11. Buxton, G.A., C.M. Care, and D.J. Cleaver, *A lattice spring model of heterogeneous materials with plasticity.* Modelling and Simulation in Materials Science and Engineering, 2001. **9**: p. 485-497.
12. Grah, M., K. Alzebdeh, P.Y. Sheng, M.D. Vaudin, K.J. Bowman, and M. Ostoja-Starzewski, *Brittle intergranular failure in 2D microstructures: Experiments and computer simulations.* Acta Materialia, 1996. **44**(10): p. 4003-4018.
13. Hassold, G.N. and D.J. Srolovitz, *Brittle fracture in materials with random defects.* Physical Review B, 1989. **39**(13): p. 9273-9281.
14. Schlangen, E. and E.J. Garboczi, *Fracture simulations of concrete using lattice models: computational aspects.* Engineering Fracture Mechanics, 1997. **57**(2-3): p. 319-332.
15. Curtin, W.A. and H. Scher, *Brittle fracture in disordered materials: A spring network model.* Journal of Materials Research, 1990. **5**(3): p. 535-553.
16. Scholz, T., G.A. Schneider, J. Munoz-Saldana, and M.V. Swain, *Fracture toughness from submicron derived indentation cracks.* Applied Physics Letters, 2004. **84**: p. 3055.
17. Barsoum, M.W., *Fundamentals of ceramics.* 2003, New York: Taylor & Francis.
18. Rice, J.R., *A path independent integral and the approximate analysis of strain concentration by notches and cracks.* Journal of Applied Mechanics, 1968. **35**(2): p. 379-386.
19. Begley, J.A. and J.D. Landes. *The J integral as a fracture criterion.* in *Fracture Toughness, Proceedings of the 1971 National Symposium on Fracture Mechanics, Part II*. 1972: ASTM.
20. Moran, B. and C.F. Shih, *Crack tip and associated domain integrals from momentum and energy balance.* Engineering Fracture Mechanics, 1987. **27**(6): p. 615-642.
21. Jin, Y. and F.G. Yuan, *Atomistic simulations of J-integral in 2D graphene nanosystems.* Journal of nanoscience and nanotechnology, 2005. **5**(12): p. 2099-2107.
22. Khare, R., S.L. Mielke, J.T. Paci, S. Zhang, R. Ballarini, G.C. Schatz, and T. Belytschko, *Coupled quantum mechanical/molecular mechanical modeling of the fracture of defective carbon nanotubes and graphene sheets.* Physical Review B, 2007. **75**(7): p. 75412.
23. McLellan, A.G., *Virial theorem generalized.* American Journal of Physics, 1974. **42**: p. 239.
24. Bencher, C.D., A. Sakaida, K.T.V. Rao, and R.O. Ritchie, *Toughening mechanisms in ductile niobium-reinforced niobium aluminide (Nb/Nb 3 Al) in situ composites.* Metallurgical and Materials Transactions A, 1995. **26**(8): p. 2027-2033.

3. Supporting figures and figure captions

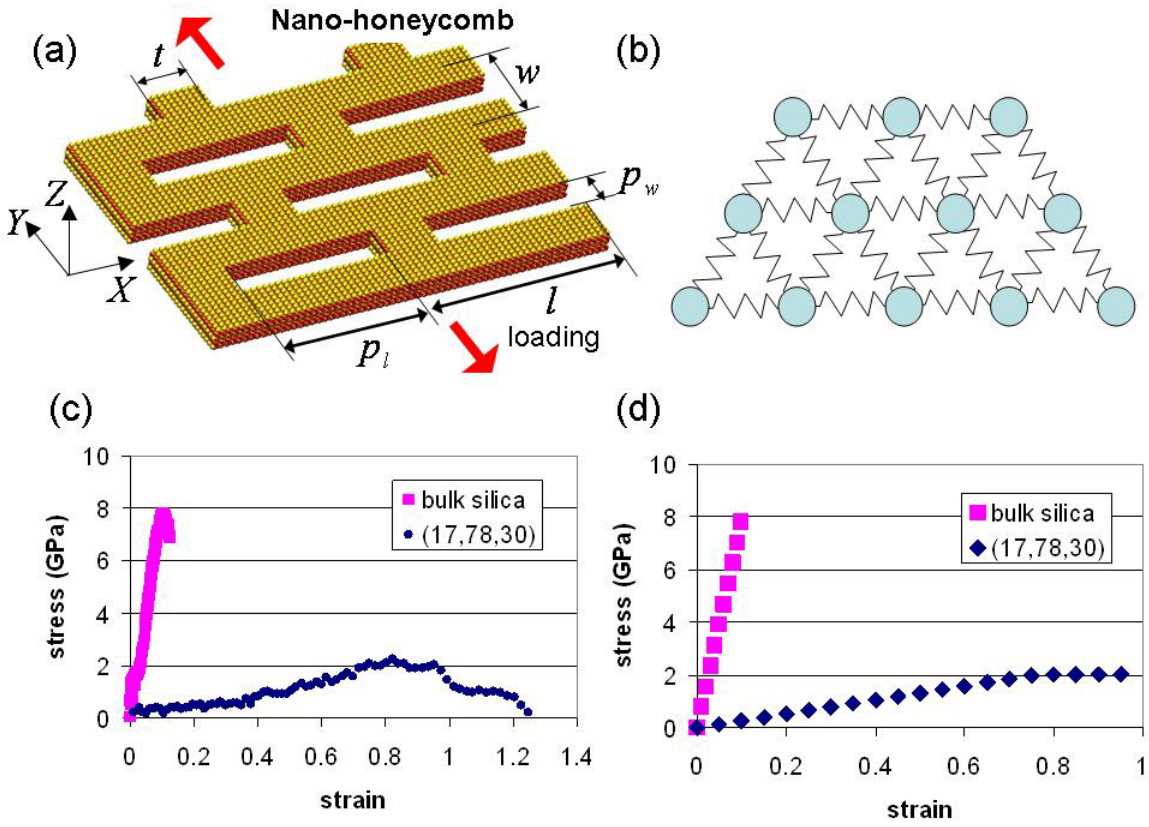

Figure S1 | Atomistic and mesoscale modeling approaches are combined here to describe the material from the nano- to the micro-scale. Parameters for the mesoscale model are derived from constitutive behavior at the nanoscale obtained using atomistic simulations. Panel (a) shows the geometry of the nano-honeycomb used as building blocks for the composite structures, panel (b) shows a section of the triangular mesh mesoscale particle-spring model setup, panel (c) show stress-strain curves obtained from atomistic simulations of a nano-honeycomb structure, and for bulk silica with a crack of the same size as the pores in the nano-honeycomb. The legend defines the nano-honeycomb structure, which is shown as (t, p_l, p_w) parameters for the structure (numerical values given in Å). The bulk silica structure shows purely brittle fracture, the nano-honeycomb structure show ductile fracture. Panel (d) shows the behavior of the mesoscale triangular mesh lattice fitted to this constitutive behavior (the agreement with the full atomistic result depicted in panel (c) is evident and provides a direct validation of the mesoscale model).

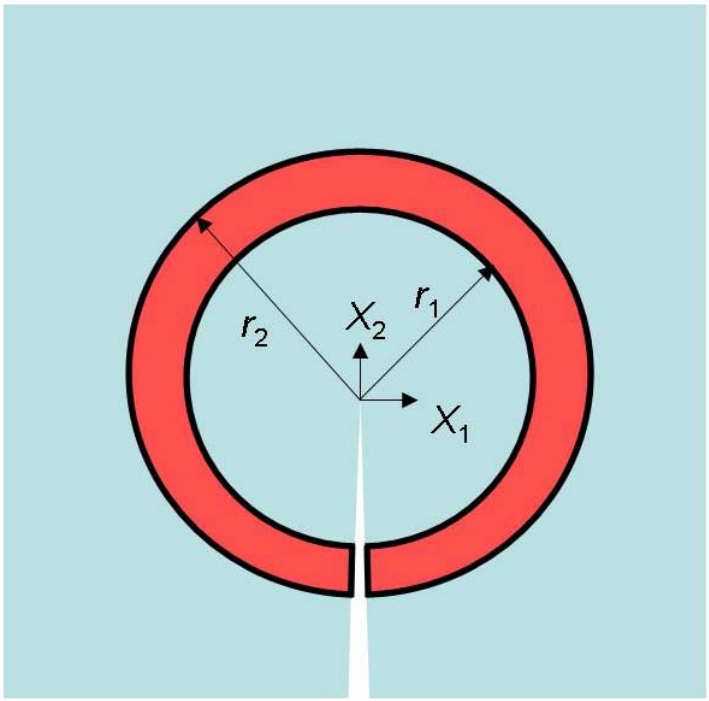

Figure S2 | The image shows the J-integral calculation for a stationary crack by the use of a domain-integral around the crack. The J-integral provides the value of the energy release rate per unit advance of the crack into the crack tip, or the resistance to crack propagation. The red/dark region shown is the domain of integration and the convergence of the J-integral is tested by taking different r_1 and r_2 regions for the same crack and specimen configuration.